

# Low Complexity Blind Phase Recovery Algorithm with Increased Robustness Against Cycle-Slips

Valery N. Rozental<sup>(1)</sup>, Deming Kong<sup>(1,2)</sup>, Benjamin Foo<sup>(1)</sup>, Bill Corcoran<sup>(1,2)</sup> and Arthur Lowery<sup>(1,2)</sup>

<sup>(1)</sup> Electro-Photonics Laboratory, Dept. Elec. & Comp. Sys. Eng, Monash University, Australia  
valery.rozental@monash.edu

<sup>(2)</sup> Centre for Ultrahigh-bandwidth Devices for Optical Systems (CUDOS), Australia

**Abstract** We present a non-data-aided recursive digital phase recovery algorithm for mQAM optical systems, which uses a priori information about the laser phase noise, and has very low computational complexity. Experimental validation shows extremely high robustness against cycle-slips.

## Introduction

Modern coherent optical systems employ digital-domain phase noise compensation. For the 16QAM modulation format, the blind phase search (BPS) algorithm, proposed in<sup>1</sup> has become a reference due to its all-feedforward hardware efficient implementation and superior performance. However, BPS suffers from high computational complexity, because it executes several phase tests in parallel. Additionally, non-data-aided phase search algorithms suffer from cycle slips, where the received signal is rotated by multiples of 90°, causing error bursts.

One way to cope with cycle slips is by using differential coding, which results in error duplication<sup>2</sup>. Several works, e.g.<sup>3,4</sup>, propose the use of pilot symbols, where the main drawback is reduced spectral efficiency. Some works, e.g.<sup>5</sup>, treat cycle slips within the decoder block. In<sup>6</sup>, a cycle slip detection and correction scheme was proposed as an add-on to a generic phase search algorithm.

In this paper, we propose and experimentally validate a recursive probability-weighted blind phase search algorithm (RW-BPS). As in BPS, RW-BPS tests several carrier phases in parallel over a noise averaging window. However, RW-BPS uses previously estimated values and tests incremental phases over a much smaller range that has non-negligible probability of occurrence. This approach allows the algorithm to maintain high precision even for a small number of test phases. Another feature of RW-BPS is that the decision error values are weighted by the a priori distribution of the corresponding phase shifts, significantly reducing, or even eliminating, cycle slip occurrences.

## Recursive weighted blind phase search

The operation principle of RW-BPS is illustrated in Fig. 1. First, incremental phase intervals are set

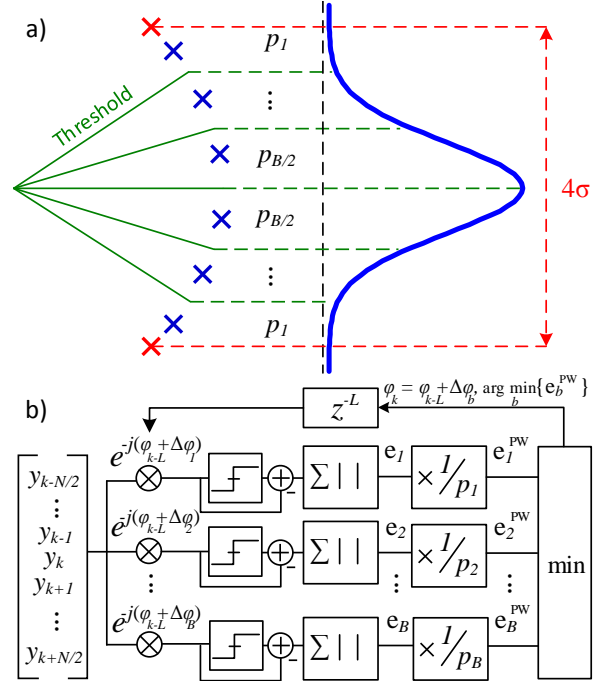


**Fig. 1:** Operation principle of RW-BPS: (a) phase interval distribution; (b) block diagram.

according to the laser parameters, symbol rate, and ASIC clock rate. Assuming perfect frequency offset compensation, incremental phase rotations are modeled as i.i.d. Gaussian random variables<sup>7</sup>  $\Delta\phi \sim N(0, 2\pi\Delta\nu T_s)$ , where  $\Delta\nu$  is the sum of carrier and local oscillator linewidths, and  $T_s$  is the symbol period. In this work, we set the non-negligible probability interval to  $4\sigma = 4\sqrt{2\pi\Delta\nu T_s}$  (which accounts for over 99.99% of  $\Delta\phi$  occurrences), and estimate  $\Delta\phi$  within this interval. The  $4\sigma$  interval is divided into  $B$  evenly-spaced test phases, where each decision region is assigned a probability according to  $\Delta\phi$  distribution. Fig. 1(a) illustrates this concept. The RW-BPS block diagram is shown in Fig. 1(b). An  $N$ -symbol vector  $[y_{k-N/2}, \dots, y_k, \dots, y_{k+N/2}]$ , where  $N$  is the size of noise rejection window, is fed in parallel to  $B$  test blocks, which apply the rotations  $\phi_{k-1} + \Delta\phi_b$ ,  $b = 1, \dots, B$ . Each block estimates the transmitted

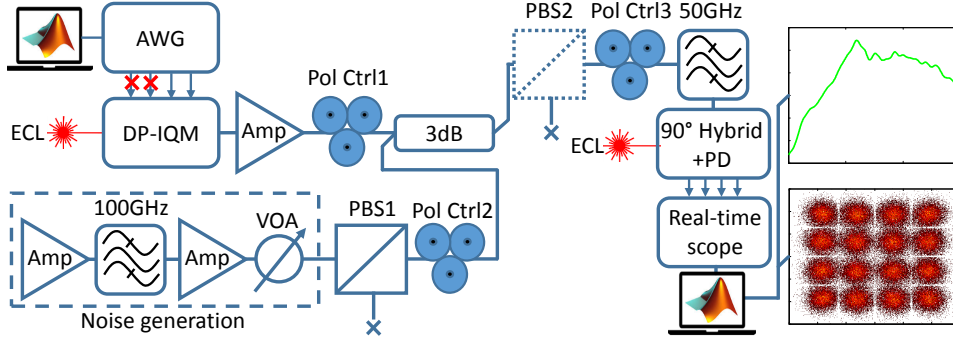


Fig. 2: Experimental setup.

symbol, yielding  $B$  estimates, for which minimum-distance errors,  $e_1, \dots, e_B$ , are computed. These errors are then divided by the corresponding *a priori* probabilities  $p_1, \dots, p_B$  of  $\Delta\phi_b$ , yielding the probability-weighted errors  $e_1^{\text{PW}}, \dots, e_B^{\text{PW}}$ . Finally,  $\phi_k$  is estimated as the value of  $\phi_{k-1} + \Delta\phi_b$  that minimizes  $e_b^{\text{PW}}$ .

One practical consideration is that transmission symbol rates in optical systems are usually higher than ASIC clock rates. Therefore, for implementation feasibility, the number of parallel processing paths,  $L$ , must be taken into account.  $L$  defines the earliest possible result,  $\phi_{k-L}$ , available at the time of  $\phi_k$  computation<sup>8</sup>, modifying the phase rotation probability:  $\Delta\phi \sim N(0, 2\pi\Delta\nu T_s L)$ , thus limiting algorithm performance.

### Experimental validation

The experimental setup is depicted in Fig. 2. At the transmit-side, a 92-GSa/s arbitrary waveform generator (AWG, 32-GHz bandwidth, 8-bit resolution), with two enabled RF outputs, corresponding to the in-phase (I) and quadrature (Q) components of a single polarization 16QAM Nyquist signal (raised cosine, roll-off 0.2) from pre-programmed digital samples. The two RF outputs drive a 35-GHz InP dual-polarization IQ modulator (DP-IQM) that modulates a 100-kHz linewidth external cavity laser (ECL). Thus, the output of DP-IQM consists of a 16QAM signal in one polarization (for reference, H-pol), and an unmodulated carrier in the orthogonal polarization (V-pol). Amplified spontaneous emission (ASE), generated by a pair of cascaded EDFAs with a 100-GHz optical filtering between the stages, is controlled by a variable optical attenuator (VOA). A polarization beam splitter (PBS1) eliminates the noise in V-pol. Next, the signal and ASE noise are combined in a 3-dB coupler, filtered by a 50-GHz optical filter, and detected with an integrated 25-GHz polarization diversity coherent receiver (ECL local oscillator, 100-kHz linewidth). An 80-GSa/s real-time oscilloscope (33-GHz bandwidth, 8-bit resolution) samples and stores the four signal tri-

butaries for offline post-processing.

Before measurements, two polarization controllers (Pol Ctrl1 and Pol Ctrl2) and additional polarization beam splitter (PBS2) were used to align signal and noise states of polarization, so that the noise is only loaded onto the 16QAM signal in H-pol, while the unmodulated carrier in V-pol remains noise-free. PBS2 was later removed from the setup for data acquisition. Additional polarization controller (Pol Ctrl3) was used to align the noisy signal and the unimpaired carrier to the receiver axes.

Carrier phase noise was extracted from the V-pol by first compensating for the frequency offset between the carrier and the local oscillator, and then applying narrowband filtering (10<sup>th</sup>-order 3-MHz Gaussian). The 16QAM signal was processed by a chain of DSP algorithms, including Gram-Schmidt orthonormalization, dynamic equalization (DE), carrier frequency offset and phase noise compensation. For DE we used non-data-aided radius-directed adaptive equalizer.

We use the Q factor as the signal quality metric, estimating it directly from the DE output prior to phase search:

$$Q[\text{dB}] = 10 \log_{10} \left( \frac{\sum_{n=1}^N |s_n|^2}{\sum_{n=1}^N (|y_n| - |s_n|)^2} \right) - 3, \quad (1)$$

where  $y_n$  is the vector of constellation points after DE, and  $s_n$  is the vector of transmitted symbols. A  $-3$  dB factor accounts for computing the errors of absolute values rather than bi-dimensional vectors. This strategy avoids inaccuracies due to constellation distortion by phase search algorithms at low SNR.

We evaluate the performance of RW-BPS and common BPS by comparing the estimated phase noise with the phase noise extracted from V-pol using mean square error (MSE) after aligning the phases to a common reference as a performance metric. Parameter values are listed in Tab. 1.

Fig. 3 shows the obtained results. Each column of the figure corresponds to a different sym-

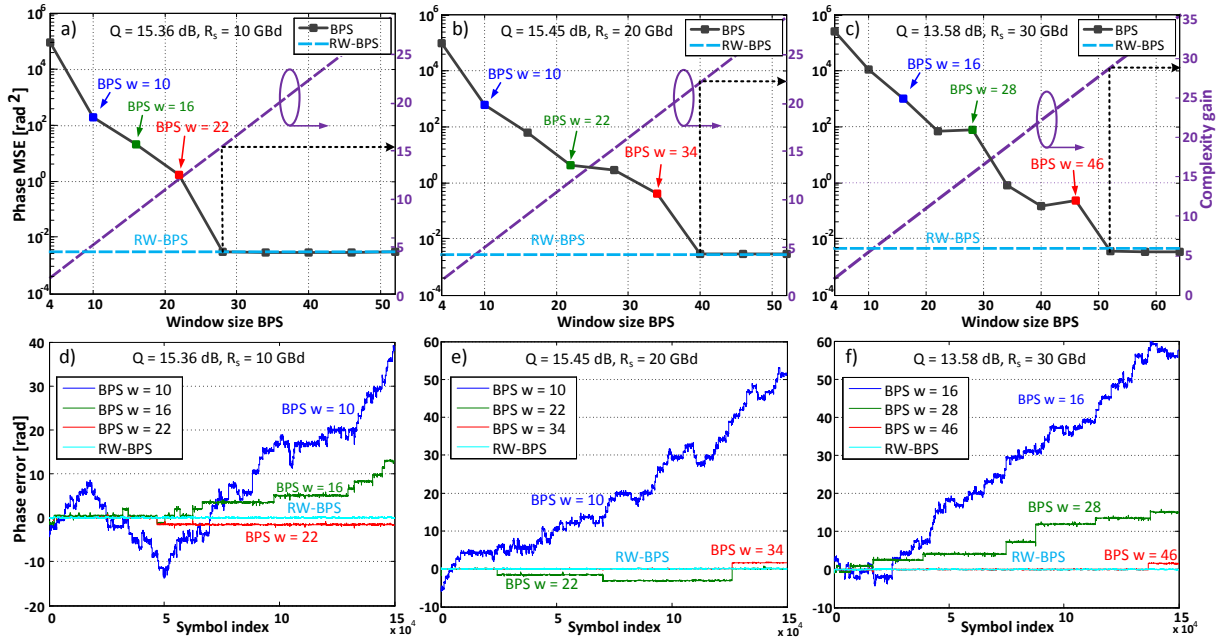


**Fig. 3:** Experimental results: (a-c) Phase MSE vs. estimator window size; (d-f) Phase error vs. symbol index, at different symbol rates. (a,d) 10 GBd @ BER=3.3 × 10<sup>-3</sup>, (b,e) 20 GBd @ BER=3.0 × 10<sup>-3</sup>, (c,f) 30 GBd @ BER=1.2 × 10<sup>-2</sup>

**Tab. 1:** BPS and RW-BPS parameters

|        | test phases, $B$ | window size, $N$ |
|--------|------------------|------------------|
| RW-BPS | 6                | 6                |
| BPS    | 20               | 4 → 64           |

bol rate,  $R_s$ , namely, 10, 20 and 30 GBd, with signal qualities around hard and soft decision FEC thresholds:  $Q = 15.36$  dB (BER  $\approx 3.3 \times 10^{-3}$ ), 15.45 dB (BER  $\approx 3.0 \times 10^{-3}$ ), and 13.58 dB (BER  $\approx 1.2 \times 10^{-2}$ ). The delays  $L$  for RW-BPS were computed as:  $L = \lceil R_s/R_{CLK} \rceil = 8, 15,$  and 22 symbols for 10, 20, and 30 GBd, where the ASIC clock rate  $R_{CLK} = 1.4$  GHz.

The figures in the upper row (Figs. 3(a-c)) show phase MSE as a function of BPS window size. Note that high MSE is related to cycle slips, as illustrated by Figs. 3(d-f). The figures also show computational complexity gain, with corresponding axes on the right-hand-side, computed as  $(N.B)_{BPS}/(N.B)_{RW-BPS}$ . Lower row figures (Figs. 3(d-f)) show phase errors for selected window sizes of BPS. The  $\pi/2$  rad jumps in the error traces correspond to cycle slips.

RW-BPS ( $N = 6, B = 6$ ) did not present cycle slips in any of the tested scenarios. For BPS, as expected, cycle slip occurrences were reduced with the window size. Comparing at the minimum window sizes where no cycle slips are observed, Figs. 3(a-c) show that for 10-, 20- and 30-GBd signals, RW-BPS has a factor 15.5, 22.2 and 28.2 less computational complexity than standard BPS. This shows, that even when taking into account the increased feedback delay due to low

ASIC clock speed, our proposed RW-BPS algorithm can significantly reduce the required complexity needed to avoid cycle slips, by accounting for the constraints of symbol-to-symbol phase drift.

## Conclusions

We have introduced a low computational complexity recursive blind phase search algorithm that uses *a priori* distribution of incremental phase rotation. Experimental results showed robustness against cycle slips.

## Acknowledgements

This work was supported by the Australian Research Council (FL130100041, CE110001018).

## References

- [1] T. Pfau et al., "Hardware-efficient Coherent Digital Receiver Concept with Feedforward Carrier Recovery for M-QAM Constellations," J. Lightwave Technol., Vol. 27, no. 8, p. 989-999 (2009).
- [2] X. Zhou, "DSP for High Spectral Efficiency 400G Transmission," Proc ECOC, Tu1E3, (2013).
- [3] H. Zhang et al., "Cycle slip mitigation in POLMUX-QPSK modulation," Proc OFC, OMJ7, (2011).
- [4] L. Liu and L. Li, "Cycle-slip correction in 100Gb/s PM-QPSK systems," Proc OFC, Th4D.2, (2014).
- [5] T. Koike-Akino et al., "Cycle Slip-Mitigating Turbo Demodulation in LDPC-coded Coherent Optical Communications," Proc OFC, M3A.3, 2014,
- [6] Y. Gao et al., "Non-data-aided and Universal Cycle Slip Detection and Correction for Coherent Communication Systems," Opt. Express, Vol. 22, no. 25, (2014).
- [7] E. Ip and J. M. Kahn, "Feedforward Carrier Recovery for Coherent Optical Communications," J. Lightwave Technol., Vol. 25, no. 9, p. 2675-2692 (2007).
- [8] M. Taylor, "Phase Estimation Methods for Optical Coherent Detection Using Digital Signal Processing," J. Lightwave Technol., Vol. 27, no. 7, p. 901-914 (2007).